Combustion and Flame 159 (2012) 817–831

Contents lists available at SciVerse ScienceDirect

Combustion and Flame

journal homepage: www.elsevier.com/locate/combustflame

Catalytic combustion of selected hydrocarbon fuels on platinum: Reactivity and hetero–homogeneous interactions

Jihad Ahmad Badra *, Assaad R. Masri

School of Aerospace, Mechanical and Mechatronic Engineering, The University of Sydney, NSW 2006, Australia

ARTICLE INFO

Article history:
Received 8 June 2011
Received in revised form 25 August 2011
Accepted 30 August 2011
Available online 8 October 2011

Keywords:
Catalytic combustion
Reactivity limits
Homogeneous and heterogeneous reactions
Micro-combustion

ABSTRACT

This paper addresses the interactions between homogeneous and heterogeneous reactions for different hydrocarbons namely, compressed natural gas (CNG), liquefied petroleum gas (LPG), butane and dimethyl ether (DME) over platinum. Experiments are performed to study the effects of varying the temperature of the incoming mixture (T_{jet}), its equivalence ratio ($\emptyset$) and the Reynolds number (Re), on the reactivity limits. Computational fluid dynamic (CFD) calculations using detailed chemical kinetics for both the platinum surface and gas phase are completed for a range of methane–air mixtures to resolve the impact of varying T_{jet}, $\emptyset$ and Re on the compositional structure of the flow. Comparison between numerical and experimental results is performed where relevant.

For flameless conditions (defined by the presence of reactions on the plate without a gaseous flame), it is found for all fuels studied here that the temperature of the platinum plate, resulting from reactions with the co-flowing fuel–air mixture, increases with increasing T_{jet} and Re. However, with CNG, the temperature of the plate peaks near stoichiometry while for LPG, butane and DME the peak occurred at richer mixtures of $\emptyset \approx 1.5$. The reactive limits for CNG, propane and DME are found to broaden significantly. Numerical simulations show very good agreement with the measured plate temperature at different equivalence ratios. The computed compositional structure confirms the existence of a flame inhibition effect due to the presence of the catalyst and shows interesting trends of some species at different Re, T_{jet} and $\emptyset$. Gas and surface chemistries seem to affect a few species such as CO, CO_2, H_2, and H_2O depending on the conditions of the co-flowing mixture. Minor species such as CH_3, CH_2O, O, HCO, and OH are largely controlled by gas-phase chemistry.

1. Introduction

It is well known that the development of micro-combustion devices as sources of power is attractive but extremely challenging. The attraction lies in the potential to provide efficient, long-life, miniature sources of heat that exploit the high energy density of hydrocarbon fuels. The heat generated could then be converted to (i) electrical energy to power portable electronic devices and hence replace bulky and short-life batteries [1,2], (ii) mechanical power such as micro-engines [3,4] and micro-turbines [5–8] to propel micro-satellites [9,10], or (iii) chemical energy in processes such as fuel reforming or the decomposition of ammonia to generate hydrogen for fuel cells [11,12]. The challenges in bringing such concepts to fruition are huge and involve cross-disciplinary issues that span many areas of research. The use of catalysts in micro-reactor devices is common to enable better control of peak temperatures and facilitate thermal management. A number of extensive reviews covering various aspects of the evolution of micro-combustion and micro-power generation devices have recently become available [1,2,13,14].

This paper is concerned with a specific but critical aspect of catalytic micro-combustion, namely the interaction between gas and surface reactions and the reactivity of platinum catalysts with different hydrocarbon fuels. This hetero–homogeneous chemistry interplay has been studied earlier by various research groups [15–22] with a focus on four fuels, namely hydrogen, carbon monoxide, methane and propane. The studies of Stefandis and Vlachos [23] were performed using a channel flow sandwiched between two parallel catalytic plates and focused on propane (C_3H_8). Other groups investigated the behavior of different fuels such as hydrogen (H_2) [24] and methane (CH_4) [25]. In Stefanidis and Vlachos [23] the bulk inlet velocity of the (lean) fuel–air mixture was varied as well as the separation between the plates and their conductivities. It was concluded that while low inlet velocities favor surface reactions, homogeneous gas chemistry continued to play a role, albeit decreasing, with decreasing gap size, to separations as low as 200 μm. Mantzaras and his group [21] studied a similar burner geometry and fuels but with the recent addition of CO/H_2–air

* Corresponding author. Address: J07 – Mechanical Engineering Building, The University of Sydney, NSW 2006, Australia. Fax: +61 2 9351 3760.
E-mail address: jihad.badra@sydney.edu.au (J.A. Badra).

0010-2180/$ - see front matter © 2011 The Combustion Institute. Published by Elsevier Inc. All rights reserved.
doi:10.1016/j.combustflame.2011.08.026

mixtures. Their detailed LIF-Raman measurements of species concentrations using LIF-Raman scattering confirm their calculations and show that the reactor stability improves at higher pressure [22].

Two other key findings emerge from the studies of Karagiannidis et al. [26]. The Lewis number effects are significant such that methane with a Le number close to unity shows "higher transverse transport towards the catalytic surface" [26] and hence wider stability limits than propane. The other finding is that the surface chemistries of CO and H_2 tend to decouple at high temperatures while for lower temperatures around 710–720 K, CO(s) coverage of the surface tends to inhibit reaction [21]. The competition between surface and gas chemistries near the catalytic surface is driven to a large extent by what Deutschmann et al. [27] refer to as the "sticking probability" of species on the surface. The decreasing sticking probabilities of H_2, O_2, and CH_4 explain the contrasting behavior of CH_4–O_2, and H_2–O_2 mixtures on a platinum surface as the percentage of oxygen in the mixture increases [27].

It is evident from these studies that in catalytic combustion, there are numerous controlling parameters that include the velocity, temperature and composition of the gas mixture as well as the properties of the reactor which include the critical dimensions where reactions occur, surface quality and thermal properties. This paper complements research reported to date by presenting a comprehensive and systematic study of the effects relating to the gas mixture namely the effects of temperature, velocity and equivalence ratio of the fuel–air mixture as key controlling parameters affecting reaction with the platinum catalyst.

Other aspects of novelty in the work presented here include: (i) the experimental investigation of four hydrocarbon fuels, namely compressed natural gas (CNG), liquefied petroleum gas (LPG), commercial butane and dimethyl ether (DME), and (ii) the use of computational fluid dynamics (CFD) with detailed chemical kinetic mechanisms for the gas and solid phases to compute the reactive structure for methane–platinum and compare with experimental measurements where relevant. The broadening in the reactive limits of these fuels over a range of inlet mixture temperatures is consistent with the findings reported earlier for propane fuels in the Swiss roll burner [28]. It should be noted that the configuration studied here is not confined but rather a free flowing mixture of fuel–air over a platinum surface. This is similar to the configuration studied by Kyritsis and co-workers [29] who investigated a platinum plate preheated with a methane/air mixture leading to a flameless reaction which was sustained on the surface. Studies of surface–gas chemistry interactions in open, unconfined flows such as those reported here and in Ref. [29] are still very relevant to the case of confined micro-reactors.

2. Experimental and numerical issues

2.1. Experimental

A schematic of the experimental apparatus is shown in Fig. 1. The 30 cm long heater (TEMPCO) consists of a ceramic shell containing a heating coil with a diameter of 8 cm surrounding a 24 mm-OD and 23 mm-ID stainless steel tube. The fuel–air mixture flows over baffle plates positioned inside the stainless steel tube to increase the heat transfer and achieve exit temperatures up to 600 °C for Reynolds numbers ranging from 250 to 1500 and with equivalence ratios that range from $\Phi = 0$ to $\Phi = \infty$. An arrangement of meshes is used within the tube and a sintered bronze plate is placed at the exit plane to keep the flow exiting the tube laminar

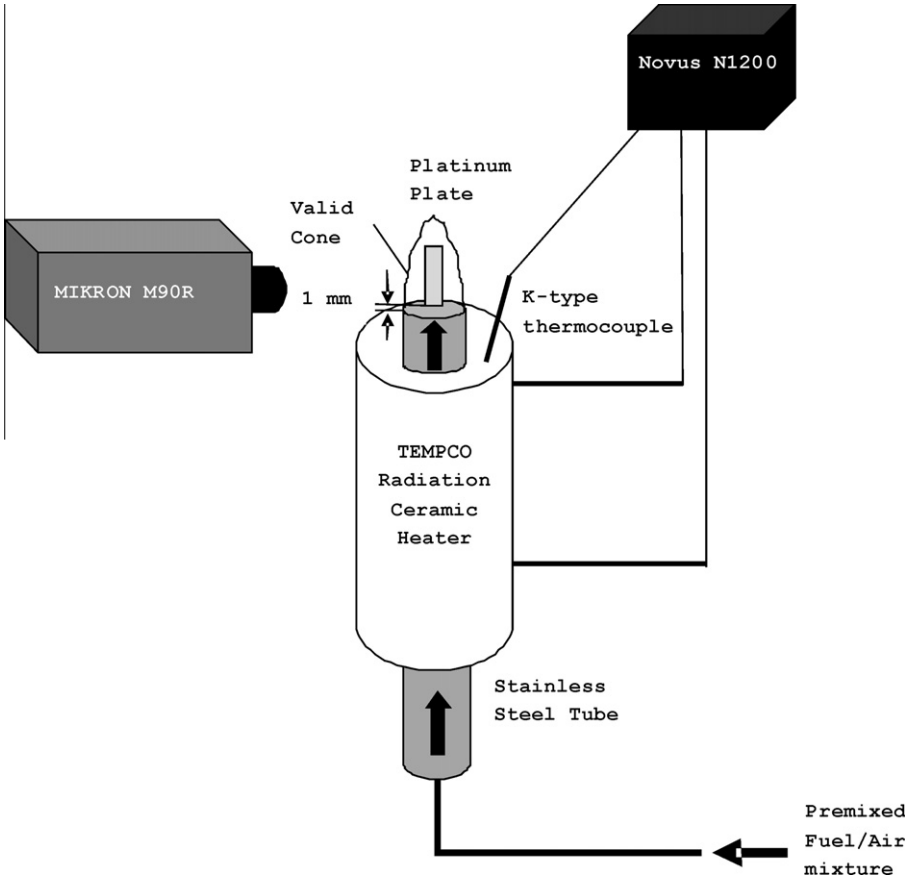

Fig. 1. Schematic of the experimental set up showing the platinum plate engulfed by gases from the jet (i.e. being within the "valid cone").

(Re < 2000) and uniform in both temperature and velocity. Gas issuing from the 23 mm-ID stainless steel tube flows over both sides of the platinum plate, which has a width of 6 mm, length of 20 mm and a thickness of 0.25 mm. This region over which flow from the tube extends without being affected by the laboratory air is referred to here as "the valid region" and this is shown schematically in Fig. 1.

Temperature measurements using a thermocouple were made at various distances from the exit plane and above the platinum plate to determine the extent of the region over which the fuel mixture is unaffected by the laboratory air. Mapping this "valid region" is important to ensure that the entire platinum plate is exposed to fuel–air mixture issuing only from the 23 mm-ID stainless steel tube. The extent of the "valid region" depends on the Reynolds number, Re_d (based on the burner diameter) of the mixture and it was found that for the platinum plate to be fully within this "valid region" a Reynolds number of more than 200 should be used. All measurements reported here ensured that the platinum plate is fully engulfed by the mixture issuing from the jet so that the results are neither dependent on the separation from the leading edge of the nozzle nor on the nozzle diameter. A PID controller (Novus N1200) is used to regulate the temperature of the mixture at the exit plane of the burner which is measured using a type-K thermocouple. The temperature of the gases exiting the tube can be varied within the range from ambient up to 600 °C. Tylan and Bronkhorst mass flow controllers are used to control the flow rates of fuels and air, respectively.

Four different fuels, namely CNG, LPG, commercial butane and dimethyl ether (DME) have been tested over platinum at various conditions. The parameters varied during the experiments are (i) the equivalence ratio, Ø of the fuel mixture co-flowing over the platinum, (ii) its temperature at the jet exit plane, T_{jet} and, (iii) its Reynolds number Re_d which is based on the 23 mm-ID of the fuel tube. Table 1 provides details of the composition of each parent fuel as obtained from the supplier and lists for each fuel the range covered for each of the three controlling parameters.

Once steady state is established for a particular flow condition, and if the fuel–air mixture does not self-ignite on the platinum surface, ignition is induced using a blow torch. If a gaseous flame is maintained immediately after ignition then the flame is forced to blow off. Subsequent to this, one of the following scenarios may then prevail:

- *Extinction*: The platinum plate cannot sustain reaction and its temperature stabilizes at that of the co-flowing mixture.
- *Flaming combustion*: Subsequent to the initial ignition and blow-off, a flame may re-ignite, propagate back and stabilize on the exit plane of the fuel tube.
- *Flameless combustion*: No flame is re-ignited subsequent to the initial blow-off but the platinum plate remains re-active. While in some cases the plate may be clearly red-hot, this does not have to be the case since surface reactions may be maintained at much lower temperatures as will be evident from the results presented here.

The surface temperature of the platinum was measured using a two-color infrared pyrometer (Mikron M90R) that covers a range between 700 °C and 2000 °C. For surface temperatures below 700 °C, an estimate is obtained by using a type-K thermocouple to measure the gas temperature just downstream the platinum plate.

2.2. Numerical

Calculations are presented here only for methane. The commercial package FLUENT-6.3.26 [30] is used to perform two-dimensional calculations for the experimental conditions studied here with the numerical domain shown in Fig. 2. The domain extends for 15 mm in the x direction and 6 mm in the y direction and has been meshed using 8600 quadratic grid cells. Monitoring the species as well as the temperature profiles resulting from a range of grids (not shown here) confirm that this mesh provides a grid-independent solution. Special care is taken near the surface because reactions start and stabilize there. To avoid high aspect ratios, the pave method is adapted for meshing. Assuming symmetry on the platinum plate, only half of the domain is calculated with one side bounded by the plate and the other by the fuel/air mixture. The inlet boundary condition is set to velocity inlet with a flat velocity profile to match the experimental conditions. The plate has a thickness of 25 mm but only half of it (12.5 mm) is modeled because of symmetry. The leading edge of the plate is located 1 mm above the jet exit plane. The boundary condition at the trailing edge of the plate (downstream) is modeled as a pressure outlet. This is justified with such configurations where flow reversal may occur within the few first time steps. The boundary opposite the plate's surface was set to symmetry since it is far away from the reaction zone. The overall extent of the numerical domain (6 mm × 15 mm) is suitable since further extensions were found to yield no change in the computed flame structure.

The DRM22 [31] mechanism is used for the volumetric reactions while Deutschmann's [32] mechanism is employed to represent surface chemistry. The GRI2.11 transport database file is used along with a comprehensive thermodynamic database accounting for the relevant gaseous and surface species. Since the flow is laminar, non-unity Lewis number is adopted with full multi-component diffusion. Gas chemistry is implemented using the ISAT algorithm with an ISAT error tolerance of 1e−6 which has been demonstrated earlier to be quite adequate for calculations involving methane [33]. Surface chemistry is implemented using direct integration. Radiation heat losses at the platinum plate are computed using the Discrete Ordinates (DO) radiation model. It is known that the emissivity of platinum (ε) varies with surface temperature and increases from $\varepsilon = 0.1$ at a temperature of 550 °C to $\varepsilon = 0.19$ at 1500 °C [34]. A fixed value for the emissivity, $\varepsilon = 0.15$ which corresponds to a temperature of 1200 °C is adopted here for convenience. This is considered to be adequate since 1200 °C is close to the average temperature experienced by the platinum during the experiments reported here. It should be noted that, as the emissivity increases, the computed peak temperature decreases but the overall shape of the computed profiles remains unchanged. The calculations for radiation are performed at every flow iteration.

The following computational process is followed for all the cases presented in this paper: For a given set of parameters

Table 1
Details of the volumetric fuel compositions and the experimental conditions covered in this paper.

Fuel	T_{jet}	Ø	Re_d	Volumetric fuel composition
CNG	21–400 °C	0.1–∞	250–1500	88.8% CH_4, 7.8% C_2H_4, 1.9% CO_2 and 1.2% N_2 with the remaining 0.3% being a mixture of propane, propene, butane and pentane
LPG	21–400 °C	0.1–∞	250–1500	95% C_3H_8, 4% C_4H_{10}, 1% C_5 + hydrocarbons
Commercial butane	21–400 °C	0.1–∞	250–1500	95.3% C_4H_{10}, 1.9% C_3H_8, 1.3% C_4H_8 and 1.3% C_5H_{12}
DME	21–400 °C	0.1–∞	250–1500	99% DME

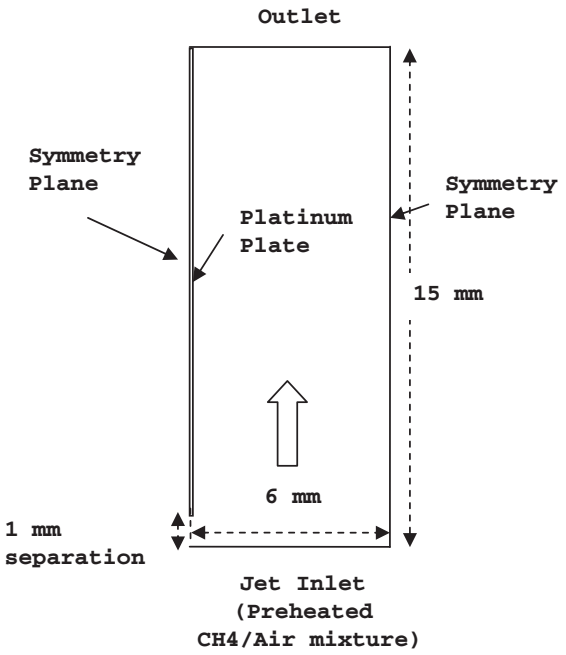

Fig. 2. Computational domain showing dimensions as well as the platinum plate used as a plane of symmetry.

(equivalence ratio, temperature and Reynolds number), a solution is first obtained for the non-reacting case, where the flow, energy and species transport equations are solved. This provides the starting flow and mixing fields to initiate calculation for the reacting cases where the platinum plate is now patched with a 1227 °C (1500 K) temperature and the chemical reactions (volumetric and surface depending on the need) are switched on. Note that the energy equation is solved within the solid plate so that heat conduction can be modeled. Second order discretization schemes are utilized for all the equations and the under relaxation parameters are modified to help achieve convergence to a stable solution. The calculations are transient and the time-step used is initially 1 μs but this is subsequently increased to 10 μs after the initial transients are washed out. After the transient solution is almost converged, the steady solver is switched on for a few iterations to reach a steady-state solution that is subsequently used for comparison with experiments.

3. Experimental results

Measurements of the peak temperature of the platinum surface, $T_{P,\max}$ are presented for the four fuel mixtures studied here, namely CNG, LPG, butane and DME. Figures 3 and 4 show profiles of the peak plate temperature ($T_{P,\max}$) versus equivalence ratio (note the logarithmic scale) plotted for Reynolds numbers ranging from 250 up to 1500. Three plots are shown for each fuel corresponding to initial approach temperatures of 21 °C, 200 °C and 400 °C. Open symbols on the figures refer to flameless conditions while filled symbols refer to flaming combustion. Solid lines refer to measurements of the platinum plate made using the pyrometer. Dashed lines refer to conditions below the threshold of the pyrometer so gas temperatures are measured using a thermocouple positioned just above the platinum plate. Note however that the extent of the plots shown in Figs. 3 and 4 do not necessarily indicate the full reactive limits. These are shown in full and further discussed in Fig. 5. The horizontal arrow, where present, marks self ignition of the fuel mixture on the platinum plate. The absence of an arrow indicates that ignition was forced using the torch as described earlier.

Figure 3 shows results for CNG and LPG and Fig. 4 reports measurements in butane and DME. While there are some similarities that are summarized later in the text, each of the four fuels shows sufficient differences to warrant a separate discussion. The following observations can be made for CNG (LHS plots of Fig. 3):

- Regardless of the temperature of the incoming CNG–air mixture T_{jet}, the maximum value of peak plate temperature occurs very close to stoichiometric and increases with increasing Reynolds number. At $T_{jet} = 21$ °C, the peak measured platinum temperature at $\Ø = 1$ increases from $T_{p,\max} = 1260$ °C to 1460 °C as the Reynolds number increases from 250 to 1500. At higher inlet temperatures of $T_{jet} = 400$ °C, the corresponding increase in $T_{p,\max}$ at $\Ø = 1$ is a bit higher and ranges from 1500 °C at Re = 250 to 1670 °C at Re = 1400.
- The lean reactive limit decreases with the increasing temperature of the incoming fuel mixture from $\Ø = 0.8$ at $T_{jet} = 21$ °C to $\Ø = 0.5$ at $T_{jet} = 400$ °C. This decrease is independent of the Reynolds number (except for a slight dependence at $T_{jet} = 21$ °C). It should be noted that for gaseous CNG–air mixtures, the lean reactive limits are 0.48 and 0.35 at mixture temperatures of 21 °C and 400 °C, respectively. This delayed reactivity for lean mixtures in the presence of platinum is also reproduced numerically (as is discussed later in this paper) and is due to the inhibiting effects of oxygen as it sticks to the platinum surface.
- For rich mixtures, the decrease in peak plate temperature occurs in two stages depending on the equivalence ratio. A region of fast decay in $T_{p,\max}$ that extends from stoichiometric to an intermediately rich equivalence ratio where $T_{p,\max}$ decreases to around 850 °C. This limit of $T_{p,\max} \sim 850$ °C is reached around $\Ø = 1.7$ at $T_{jet} = 21$ °C regardless of Re. However, at higher values of T_{jet}, a dependence on Reynolds number is observed so that at $T_{jet} = 400$ °C the 900 °C limits are reached at $\Ø = 1.7$ at Re = 250 and $\Ø = 3.0$ at Re = 1400. For richer mixtures, the decrease in $T_{p,\max}$ is minimal (region of slow decay in $T_{p,\max}$) and seems to be largely independent of the Reynolds number and even T_{jet}. This is expected since these fuel-rich conditions are dominated by surface chemistry and the surface sites are expected to be saturated with carbon atoms, C(s).

The behavior of LPG over platinum is significantly different from CNG as can be clearly seen from the plots presented on the RHS of Fig. 3. The following observations are made, noting differences and similarities between LPG and CNG fuels:

- Unlike CNG, and for flameless conditions, the tendency for LPG–air mixtures over platinum is to reach peak temperatures at a rich (rather than stoichiometric) equivalence ratio of around $\Ø = 1.5$. This is true regardless of the Reynolds number or even the temperature of the incoming mixture as is evident from the profiles shown at $T_{jet} = 21$ °C and from the only flameless condition obtained at $T_{jet} = 200$ °C and Re = 250.
- As marked by the solid circles on the RHS of Fig. 3, flaming combustion occurs for LPG–air mixtures at $T_{jet} = 200$ °C and Re = 750 and 1400 and for all Reynolds numbers at $T_{jet} = 400$ °C. Note here that, as expected, flaming combustion occurs within the flammability limits of the gaseous mixtures only and flameless conditions are resumed outside these limits. Also, when flaming combustion occurs, the peak plate temperature is dictated by the gas temperature and is independent of Reynolds number since the stain rates are very low in this flow configuration. Values of $T_{p,\max} = 2070$ °C and 2160 °C are measured at stoichiometric for $T_{jet} = 200$ °C and 400 °C, respectively. Note also that these flaming conditions have not been observed in the CNG flames.

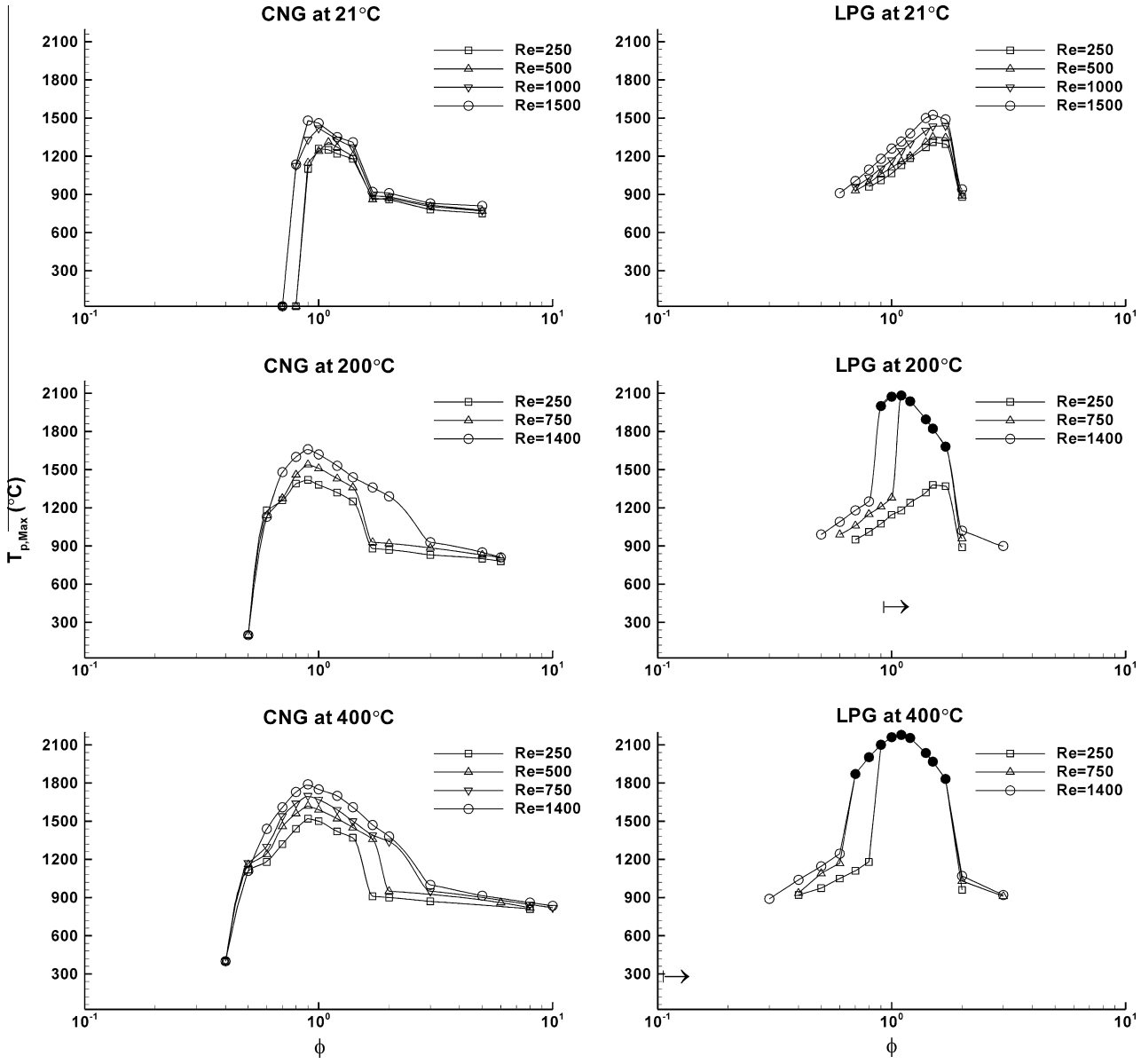

Fig. 3. Maximum measured surface temperature plotted versus equivalence ratio, Ø (on a logarithmic scale) for CNG and LPG fuels at different values of T_{jet} and Re.

- As indicated by the arrow on some RHS plots of Fig. 3, self-ignition occurs for certain mixtures depending on the temperature, equivalence ratio and Reynolds number. This is another difference with CNG–air mixtures where self-ignition did not occur at any of the tested conditions. For LPG–air mixtures with T_{jet} = 400 °C self-ignition occurs for mixtures with Ø > 0.1 regardless of the Reynolds numbers while for T_{jet} = 200 °C self ignition occurs at Ø > 0.9 regardless of the Reynolds number.
- A point of similarity with CNG–air is that, for flameless conditions, the peak platinum temperature increases with Reynolds number (but the peak occurs at a different equivalence ratio for CNG and LPG fuel mixtures). For LPG–air at T_{jet} = 21 °C, values of $T_{p,max}$ measured at the peak condition of Ø = 1.5 range from 1310 °C at Re = 250 to 1520 °C at Re = 1500.

Figure 4 shows profiles of $T_{P,max}$ versus equivalence ratio, Ø for butane and DME plotted at similar conditions to those shown in Fig. 3 for CNG and LPG. The common feature for all four fuels is the fact that, for flameless conditions, the peak surface temperature, $T_{P,max}$ increases with Reynolds number. This feature is consistent with earlier studies of micro-reactors performed by Stefanidis and Vlachos [23] and is caused by the increased platinum reactivity due to the injection of additional fuel at higher Reynolds numbers. While this is one of the few common features noted between the four fuels, many similarities are observed in the trends of LPG, butane and DME (but not CNG) as noted here:

- In flameless combustion modes, peak surface temperatures occur at rich equivalence ratios of around Ø ≈ 1.5 for all three fuels. This is clear evidence that the platinum surface chemistry is controlling at these conditions.
- Flaming combustion occurs at selectively higher temperatures depending on the fuel-mixture and the Reynolds numbers. For butane and DME, a single condition of flaming combustion occurs at T_{jet} = 21 °C, Re = 1500 and an equivalence ratio of 1.4 and 1.2 for butane and DME, respectively. However, for T_{jet} = 200 °C butane sustains a flame only at Re = 1500 within the range 1.1 < Ø < 1.7 while for DME ignites a flame at all Reynolds numbers albeit with a decreasing range of lean equivalence ratios (the lean limits for flaming combustion are 1.1, 1,

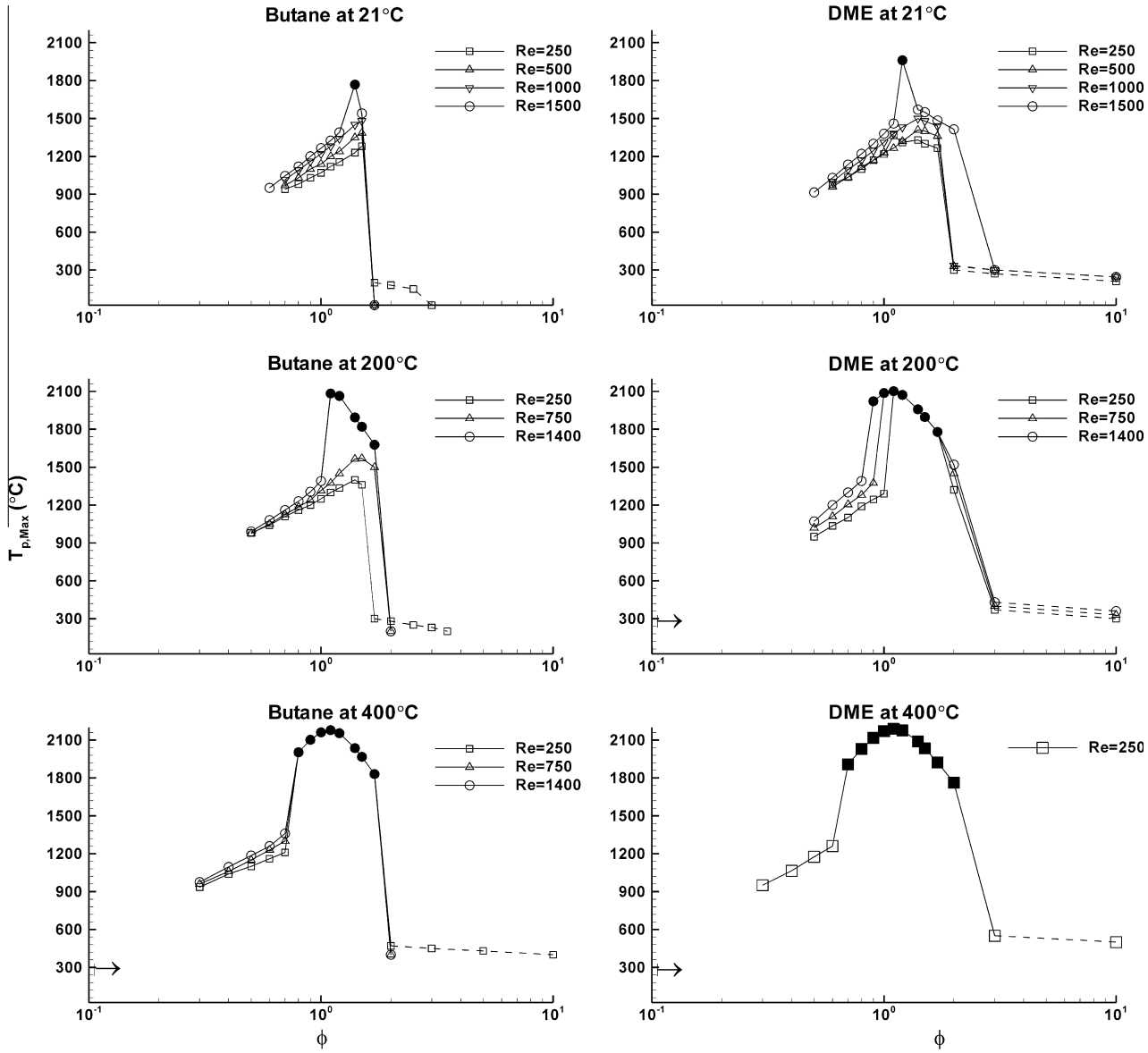

Fig. 4. Maximum measured surface temperature plotted versus equivalence ratio, Ø (on a logarithmic scale) for butane and DME fuels at different values of T_{jet} and Re.

and 0.9 at Re = 250, 750 and 1400, respectively). At T_{jet} = 400 °C, both butane and DME stabilize flames at all Reynolds numbers and within a fixed range of equivalence ratios which are $0.8 < Ø < 1.7$ for butane and $0.7 < Ø < 2$ for DME.

- As for LPG–air, self ignition occurs at high inlet temperatures for both butane and DME. However, it is clear that DME is much more reactive than both butane and LPG. As T_{jet} rises to 200 °C, self ignition of DME–air mixtures occurs at all Reynolds numbers for $Ø > 0.1$. This is also true for T_{jet} = 400 °C. Another indicator of the higher reactivity of DME is that at rich mixtures, the transition from the region of fast decay to the region of slow decay in $T_{p,max}$ moves from Ø = 2 at T_{jet} = 21 °C to Ø = 3 at 200 °C and 400 °C.

The reactive limits for the four fuels studied here are presented in Fig. 5 as plots of equivalence ratio versus Reynolds number for various fuel mixture temperatures, T_{jet} (except for DME where only one temperature of T_{jet} = 21 °C is presented). Note that both axes show logarithmic scales. Lean and rich reactive limits ($Ø_L$, $Ø_R$) are presented for each value of T_{jet}. It should be noted that these limits are determined here from temperature measurements obtained using either the pyrometer (for the temperature range 700 °C to 2000 °C), or a thermocouple placed on top of the platinum plate. Therefore, reported temperatures outside the range of 700 °C to 2000 °C are for the gas phase rather than the platinum surface. The reactive limits are defined by the condition when the temperature rise decreases to almost zero, i.e. when the temperature of the platinum (or the gas downstream of it, as measured by the thermocouple) drops to that of the incoming fuel mixture stream.

For all fuels studied here, the reactive limits are generally broader than those obtained for the gas-phase alone and may extend to extreme conditions depending on the fuel. Selected lean and rich reactive limits obtained experimentally for four fuels are shown in Table 2 for a range of temperatures and for two Reynolds numbers, namely Re = 250 and 1000. Also shown in Table 2 for comparison are the corresponding gaseous lean and rich flammability limits ($Ø_{L,gasphase}$ and $Ø_{R,gasphase}$). These are either obtained from the literature or estimated using a correlation by Zabetakis [35]. The following additional observations are noted:

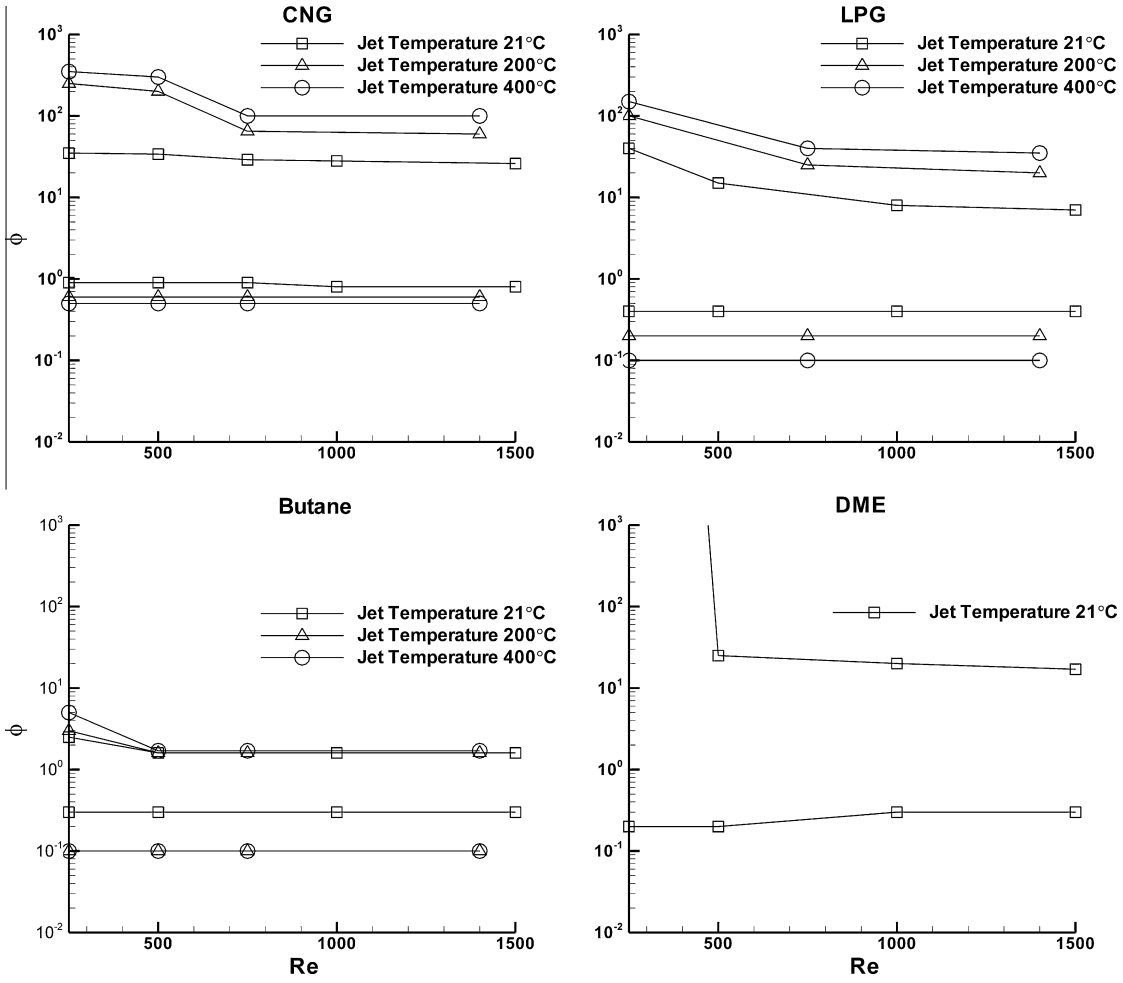

Fig. 5. Plots of Ø versus Re on a log–log scale showing the experimental lean and rich reactive limits of different fuels–air mixtures over platinum and for different values of T_{jet}.

Table 2
Experimental lean and rich flammability limits obtained on the platinum surface for the four fuel–air mixtures at different temperatures and for Re = 250 and Re = 1000. Also shown here are the limits corresponding to the gaseous-only mixtures.

Mixture	Temperature (°C)	$Ø_{L,experiment}$ Re = 250	$Ø_{L,experiment}$ Re = 1000	$Ø_{L,gasphase}$	$Ø_{R,experiment}$ Re = 250	$Ø_{R,experiment}$ Re = 1000	$Ø_{R,gasphase}$
CNG–air	21	0.9	0.8	0.48	35	28	1.4
	200	0.6	0.6	0.42	250	63	1.6
	400	0.5	0.5	0.35	350	100	1.8
LPG–air	21	0.4	0.4	0.5	40	8	2.3
	200	0.2	0.2	0.44	100	23	2.6
	400	0.1	0.1	0.37	150	37	2.9
Butane–air	21	0.3	0.3	0.56	2.5	1.6	2.6
	200	0.1	0.1	0.49	3	1.6	2.9
	400	0.1	0.1	0.41	5	1.7	3.3
DME–air	21	0.2	0.3	0.49	∞	20	3.8

- The lean reactive limits, $Ø_L$ are generally independent of the Reynolds number and decrease with increasing temperature of the mixture. This statement is true for gas phase mixtures and appears to imply that gas-phase chemical kinetics play a significant role in determining $Ø_L$. However, CNG fuel behaves differently compared to the other fuels where, $Ø_L$, in the presence of platinum, is higher than $Ø_L$ for gaseous CNG–air mixtures as shown in Table 2. On the other hand, LPG, butane and DME show the opposite trend where, $Ø_L$ dictated by the platinum is always less than the corresponding gaseous lean flammability limit ($Ø_{L,gasphase}$).
- The rich reactive limits, $Ø_R$ vary wildly between different fuels as also noted from the graphs shown in Fig. 5 and from the values shown in Table 2 for representative Reynolds numbers of 250 and 1000. It is clear also from the values of $Ø_R$ shown in Table 2 that, except for butane, these are much higher than

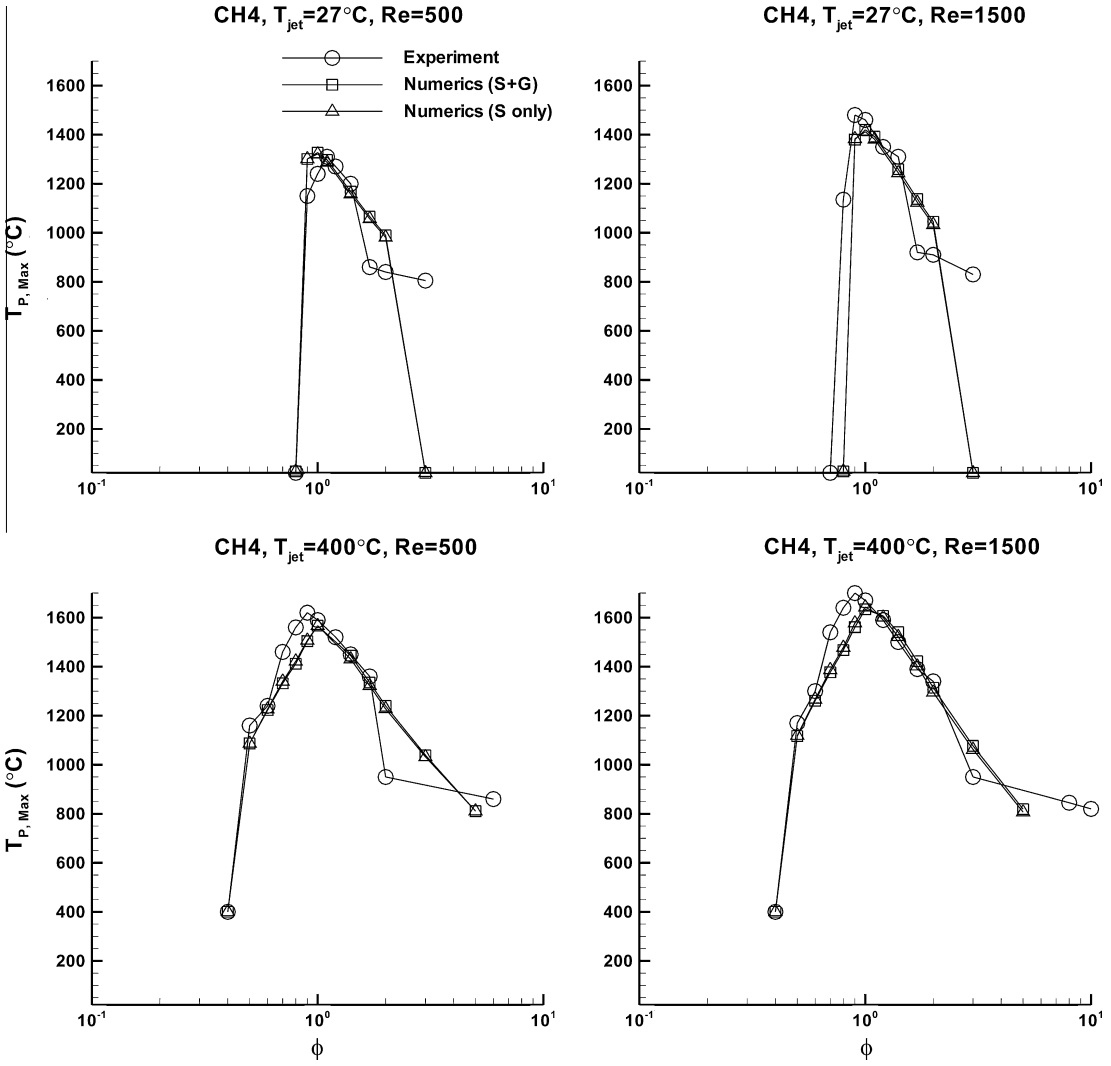

Fig. 6. Maximum measured surface temperature plotted versus equivalence ratio, $\emptyset$ (on a logarithmic scale) for methane–air mixtures over platinum: Numerical predictions for "S + G" and "S only" compared with experimental data for various flow conditions.

the rich limits computed for gaseous mixtures of the same fuel and at the same temperature. These results, at least for LPG, are consistent with the findings of Maruta et al. [28] and Ahn et al. [36] who reported a significant increase in the reactive limits for propane when platinum is introduced in the Swiss Roll reactor. The proximity of the gaseous and surface $\emptyset_R$ limits for butane needs further study and may be due to the platinum surface becoming saturated with carbon atoms, C(s) so that gaseous chemistry dominates.

- The trend observed for CNG, LPG and DME (not shown here) is for $\emptyset_R$ to increase at higher values of T_{jet} regardless of the Reynolds number. Conversely, butane shows a somewhat contradictory behavior, where $\emptyset_R$ is independent of T_{jet} at high Reynolds numbers (Re > 500). This is even inconsistent with the trends obtained for the gaseous butane–air mixtures (see Table 2) and such behavior requires further investigation. However, at low Reynolds numbers (Re = 250) $\emptyset_R$ of butane increases with T_{jet}.
- At low Reynolds numbers (say less than 300), values of $\emptyset_R$ start off generally a bit higher and decrease slowly to plateau at Re $\sim$ 700 and higher. This is true for all fuels shown here except DME where the increase in $\emptyset_R$ at low Reynolds numbers (Re < 400) is somewhat exponential since pure DME at 21 °C reacts on platinum at Re = 250. This threshold increases to Re = 800 when DME is heated to 200 °C (not shown here). These findings support the view that DME is the most reactive of the four fuels tested here.

4. Numerical results

To confirm the validity of the numerical approach, this section starts by comparing the measured and computed temperatures for a selection of cases. Note that CNG is conveniently used throughout as equivalent to pure methane. Given that boundary-layer thickness of about 1 mm closer to the leading edge is comparable to the width of the plate, the two-dimensionality of the boundary layer may be questioned. To alleviate this concern, an experiment was conducted with a wider strip of 20 mm and this reproduced very similar results to the 6 mm strip within the region of interest reported here (within at least 5 mm from the leading edge). This confirms that the boundary layer may be treated as two-dimensional and hence the 2D-calculations reported here are well justified. Next, some details of the compositional structure are presented. For each case, calculations are repeated with the gaseous reactions being disabled so that only platinum surface chemistry is active. Such cases are labeled as "Surface" (or with

subscript S) as opposed to the standard calculations that employ both gas and surface chemistry (labeled with a subscript S + G, or Surface + Gas). Such dual calculations highlight the importance of the homogeneous and heterogeneous chemistries in the methane–platinum cases studied here.

Figure 6 shows a comparison between the measured and computed maximum plate temperature, $T_{p,\max}$ for four methane–air cases, namely: T_{jet} = 27 °C and 400 °C, Re = 500 and 1500. For each case, two calculations are presented for the surface (S) as well as surface + gas (S + G) conditions. Results are plotted versus equivalence ratio, Ø (on a logarithmic scale). All calculations show no difference between the computed temperatures from the S and S + G cases implying that surface reactions are dominant at least for the main heat release. Profiles of computed species concentration

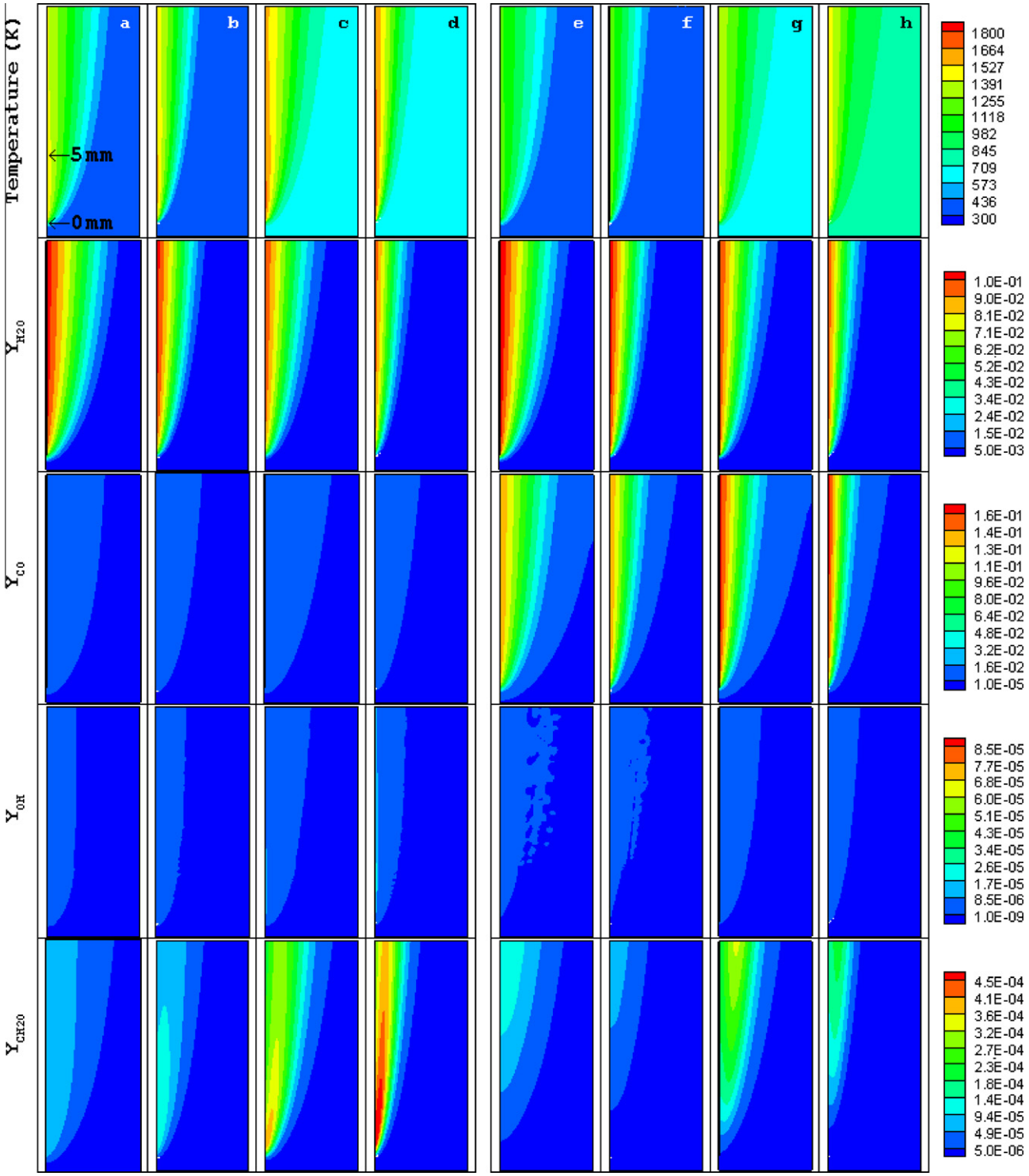

Fig. 7. Contours of temperature, species mass fractions of H_2O, CO, OH and CH_2O for (a) T_{jet} = 27 °C, Ø = 0.9 and Re = 500, (b) T_{jet} = 27 °C, Ø = 0.9 and Re = 1500, (c) T_{jet} = 400 °C, Ø = 0.9 and Re = 500, (d) T_{jet} = 400 °C, Ø = 0.9 and Re = 1500, (e) T_{jet} = 27 °C, Ø = 2 and Re = 500, (f) T_{jet} = 27 °C, Ø = 2 and Re = 1500, (g) T_{jet} = 400 °C, Ø = 2 and Re = 500, and (h) T_{jet} = 400 °C, Ø = 2 and Re = 1500, where both surface and gaseous reactions are enabled.

shown later highlight some differences and hence some contribution of the gas-phase chemistry.

Agreement with the measured peak surface temperatures is also very good particularly for methane–air mixtures with equivalence ratios less than $\emptyset \sim 1.4$. The lean reactive limits, which are higher than those of gaseous methane–air mixtures (see Table 2), are also well-reproduced confirming that the surface chemistry is inhibiting reactions. The reasons for such inhibition at these lean conditions are due to the oxygen's affinity (or sticking probability [27]) to the platinum being stronger than methane. This saturates the platinum surface with oxygen hence leaving no vacant sites for the methane to adsorb and react. At richer equivalence ratios, calculations show a continuous decrease in $T_{p,\max}$ and fail to reproduce dual regions of fast and slow decay in $T_{p,\max}$ (with a transition at $\emptyset \sim 1.7$) which has been observed experimentally. Another discrepancy lies in the extent of the rich reactive limits where at $T_{jet} = 27\ ^\circ C$, calculations yield an extinguished condition at $\emptyset \sim 3$ while experiments show a rich limit of $\emptyset \sim 35$ (see Fig. 5). This difference may also be as significant at higher values of T_{jet} although it is harder to see from the results shown in Fig. 6. Such discrepancy may well be due to the extent of surface coverage of vacant sites (Pt(s)) with carbon, C(s).

Shown in Fig. 7, in false colors, are computed contours of temperature and the mass fractions of H_2O, CO, OH and CH_2O representing the spatial distribution over almost the entire region adjacent to the platinum plate. Calculations include both surface and gas chemistries (S + G) and the range of values computed for each scalar are indicated on the color bar on the far right of the page. Each image covers a spatial distance of 16 mm (vertically) and 6 mm horizontally. The platinum plate corresponds to the vertical axis with the leading edge at 1 mm above the base and the horizontal axis represents distance orthogonal to the plate. Calculations are shown for two values of T_{jet} (27 °C and 400 °C), Reynolds number (Re = 500 and 1500) and equivalence ratios ($\emptyset$ = 0.9 and 2.0). Horizontal rows of images correspond to a particular computed parameter (temperature and species mass fractions) while columns refer to a particular set of conditions (T_{jet}, $\emptyset$ and Re).

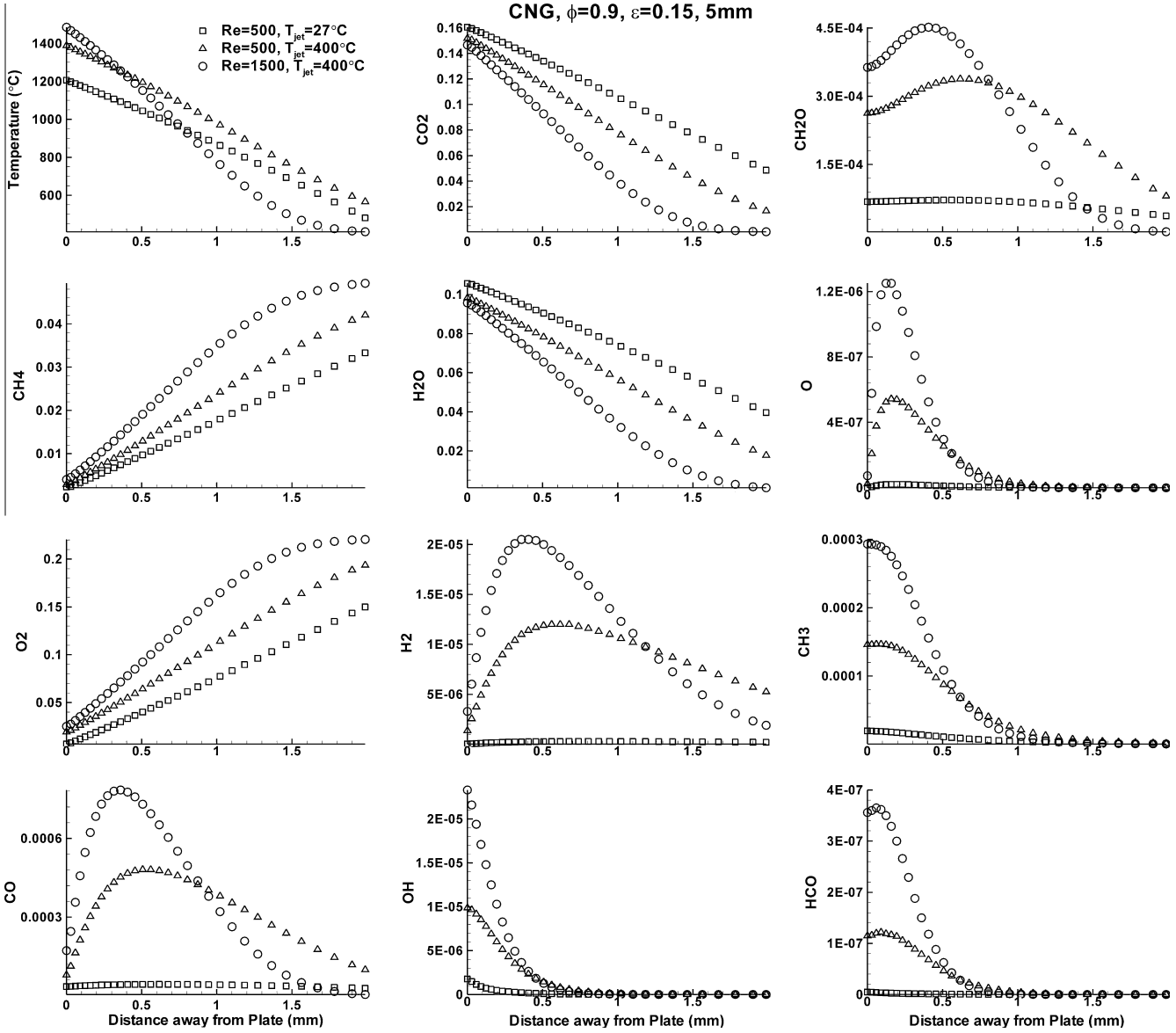

Fig. 8. Transverse profiles of temperature and species mass fractions computed for CH_4–air over platinum at $\emptyset$ = 0.9 and for a range of values of T_{jet} and Re as indicated in the inset.

A common feature to almost all the images shown in Fig. 7 is that reaction is generally initiated within at the leading edge of the platinum and the boundary layer formed on the plate grows in thickness with distance. Just downstream of the leading edge, the temperature and composition fields become uniform and do not change further with axial distance. It is also notable that the computed peak mass fraction of water (second row of images) remains almost constant regardless of the equivalence ratio, Re and T_{jet}. While the mass fraction of CO (third row of images) is almost unaffected by changes in Re and T_{jet}, it increases significantly for rich mixtures with peak values of Y_{CO} changing from 0.0002 at $\emptyset = 0.9$ to 0.146 at $\emptyset = 2.0$ for $T_{jet} = 27$ °C and Re = 500. The mass fraction of OH is affected somewhat by equivalence ratio, Re and T_{jet} but the changes are hard to quantify from the shown images and are discussed later in this paper. Formaldehyde, CH_2O increases in magnitude with increasing Re and T_{jet}. For richer mixtures ($\emptyset = 2$), the initiation of CH_2O is delayed downstream of the leading edge of the plate but the peak mass fraction of CH_2O also increases with rising T_{jet}.

Figures 8 and 9 show further details of the compositional structure within the boundary layer at two equivalence ratios of $\emptyset = 0.9$ and $\emptyset = 2$, respectively. Each figure shows transverse profiles for temperature and the mass fraction of eleven species (CH_4, O_2, CO, CO_2, H_2O, H_2, OH, CH_2O, O, CH_3, HCO) plotted along a line 5 mm from the leading edge of the plate (this location is marked in Fig. 7a). This position is deemed to be representative of the entire boundary layer as can be seen from the contours shown in Fig. 7. The calculations shown here employ both surface and gas chemistries (S + G). Each plot of Figs. 8 and 9 shows three profiles plotted versus distance from the surface of the plate and each profile corresponds to a different combination of Reynolds number and T_{jet} as shown in the legend.

The temperature profiles confirm earlier findings showing that the temperature of the plate increases with increasing T_{jet} and Re reaching a value of 1600 °C at $T_{jet} = 400$ °C and Re = 1500. This is well above the ignition temperature of methane and yet no flaming combustion is established because both O_2 and CH_4 are consumed on the platinum to produce H_2O and CO_2. This is evident from Fig. 8

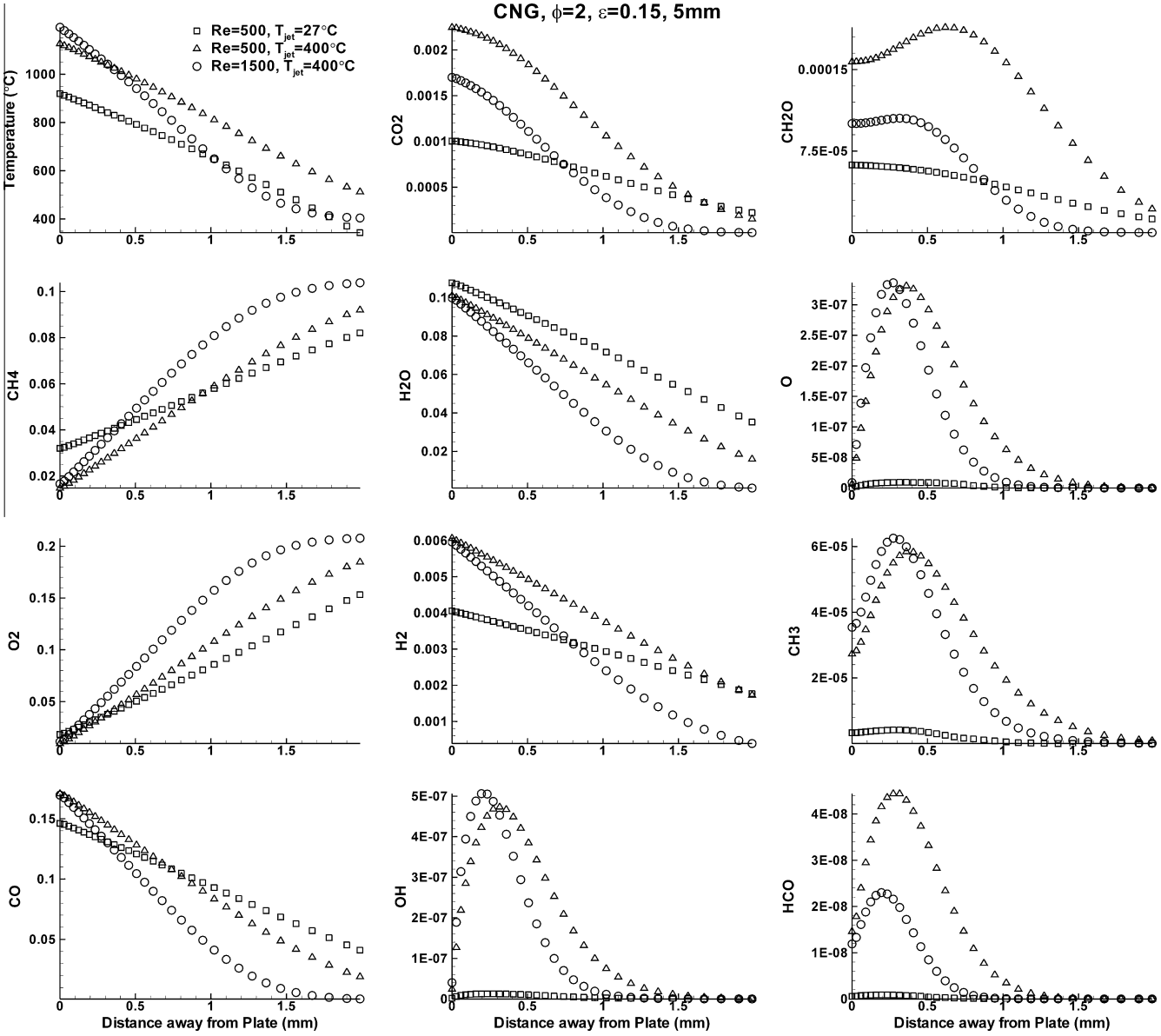

Fig. 9. Transverse profiles of temperature and species mass fractions computed for CH_4–air over platinum at $\emptyset = 2$ and for a range of values of T_{jet} and Re as indicated in the inset.

which shows for Ø = 0.9 mass fractions of about 0.1 and 0.15 for H_2O and CO_2, respectively. The rate of consumption of O_2 and CH_4 increases with increasing T_{jet} and Re as reflected in the steeper slopes and this phenomenon of flame inhibition due to the presence of platinum is consistent with what has already been reported by Bui et al. [37]. It is worth noting that for rich mixtures (Ø = 2), and at T_{jet} = 27 °C and Re = 500 (Fig. 9), the platinum surface becomes saturated so that a residue mass fraction of methane Y_{CH_4} = 0.03 is now seen on the surface and the conversion efficiency to H_2O and CO_2 is reduced as reflected by the decrease in their respective mass fractions.

The behavior of other minor species shown in Figs. 8 and 9 is very interesting. For lean mixtures of Ø = 0.9 (Fig. 8), radicals such as O, OH, CH_3 and HCO form very close to or on the surface and decay very quickly, within about 0.5 mm from the surface to yield peaks in CO, H_2 as well as formaldehyde CH_2O. This behavior is most noticeable for T_{jet} = 400 °C and Re = 1500 with the peaks decreasing at Re = 500 and decreasing much further at T_{jet} = 27 °C and Re = 500 so that at this latter condition the conversion to H_2O and CO_2 is at its highest state. Formaldehyde maintains its presence on the surface yet peaks at some distance of about 0.5 mm at T_{jet} = 400 °C. This is driven by the varying production/consumption rates of CH_2O which start negative on the surface (consumption) but change to positive (production) 0.5 mm away from the surface. Increasing the temperature from T_{jet} = 27 °C to 400 °C (at Re = 500) changes the consumption rate at the surface by an order of magnitude, from −0.012 kg/m^3 s to −0.12 kg/m^3 s, respectively. However, at 0.5 mm from the surface, the production rate of CH_2O increases by 20 times from 0.002 kg/m^3 s to 0.04 kg/m^3 s hence explaining the higher mass fractions of formaldehyde at this condition.

For rich mixtures with Ø = 2 (Fig. 9), the abundance of methane close to the surface causes higher site occupancy and hence poorer conversion to stable species such as H_2O and CO_2. Instead, CO and H_2 are now much more abundant than for the lean case (Ø = 0.9, Fig. 8) and peak right on the surface. The peak mass fraction of CO_2 is also reduced drastically from around 0.15 for Ø = 0.9 to less than 0.0003 for Ø = 2. An interesting shift in trend is also observed for CH_2O and HCO in Fig. 9, where the mass fractions of those species increase with increasing T_{jet} and reduce with increasing Re.

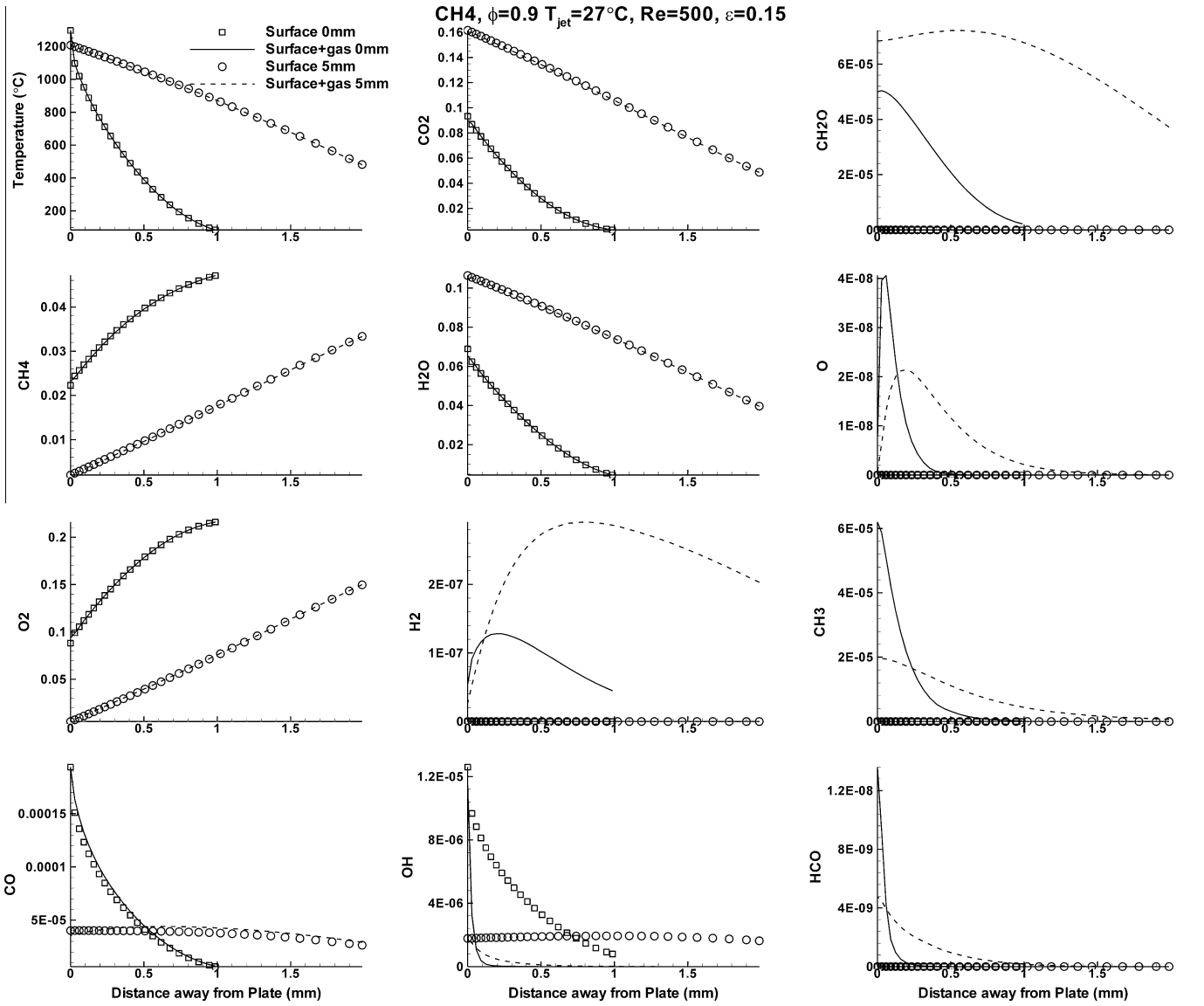

Fig. 10. Transverse profiles of temperature and species mass fraction computed for T_{jet} = 27 °C, Ø = 0.9 and Re = 500. Profiles are shown for two downstream locations (0 mm and 5 mm) using surface only or surface + gas reactions as marked on the inset.

The remaining minor species shown in Fig. 9, (OH, O and CH_3) experience significant change when T_{jet} increases from 27 °C to 400 °C but remain constant with increasing Reynolds numbers.

4.1. Homogeneous/heterogeneous reactions

Calculations presented in Fig. 6 show that the peak surface temperature of the platinum surface $T_{p,max}$ is mainly controlled by surface chemistry since it remains unchanged when the gas chemistry is numerically switched off. This section provides a more thorough analysis of the interplay between surface and gas reaction and their impact on the compositional structure of the flow near the platinum surface. Calculations using surface only (S) and surface + gas (S + G) chemistry are repeated for lean and rich methane flows with Ø = 0.9 and Ø = 2, at two inlet temperatures, T_{jet} = 27 °C and 400 °C and two Reynolds numbers (Re = 500 and 1500).

Figures 10–12 show sample results for only three cases with Re = 500 and (i) Ø = 0.9, T_{jet} = 27 °C, (ii) Ø = 0.9, T_{jet} = 400 °C, and (iii) Ø = 2, T_{jet} = 27 °C. Each figure shows profiles of the computed temperature and mass fraction of eleven species (CH_4, O_2, CO, CO_2, H_2O, H_2, OH, CH_2O, O, CH_3, HCO) plotted transverse to the platinum plate starting from two locations, the leading edge (0 mm) and 5 mm from leading edge. The locations of these profiles are shown by black arrows on the top LHS of Fig. 7. They are chosen here to illustrate the spatial evolution of the boundary layer noting that the location of 5 mm from the leading edge of the plate is representative of the remaining boundary layer (see Fig. 6). For each species, and for each of the two locations on the plate two profiles are shown for the (S + G) and (S) calculations.

It is shown from Fig. 10 (Ø = 0.9, T_{jet} = 27 °C, and Re = 500) that temperature and the computed mass fractions of CH_4, O_2, CO, CO_2 and H_2O are almost fully controlled by surface chemistry given that the profiles from S and S + G calculations almost overlap (except for a slight deviation in the CO profiles). However, H_2, OH, CH_2O, O, CH_3 and HCO show huge differences confirming that gas chemistry plays a key role in their formation. This is expected for CH_2O, O and HCO which are not part of the surface mechanism anyway. The methyl radical, CH_3 is part of the platinum chemistry but reacts only on the surface and never desorbs as a gaseous species. Hydrogen mass fraction is zero on the plate's surface and peaks some 0.5–1.0 mm away but is formed by virtue of homogeneous chemistry. Conversely, OH mass fraction at the leading edge is

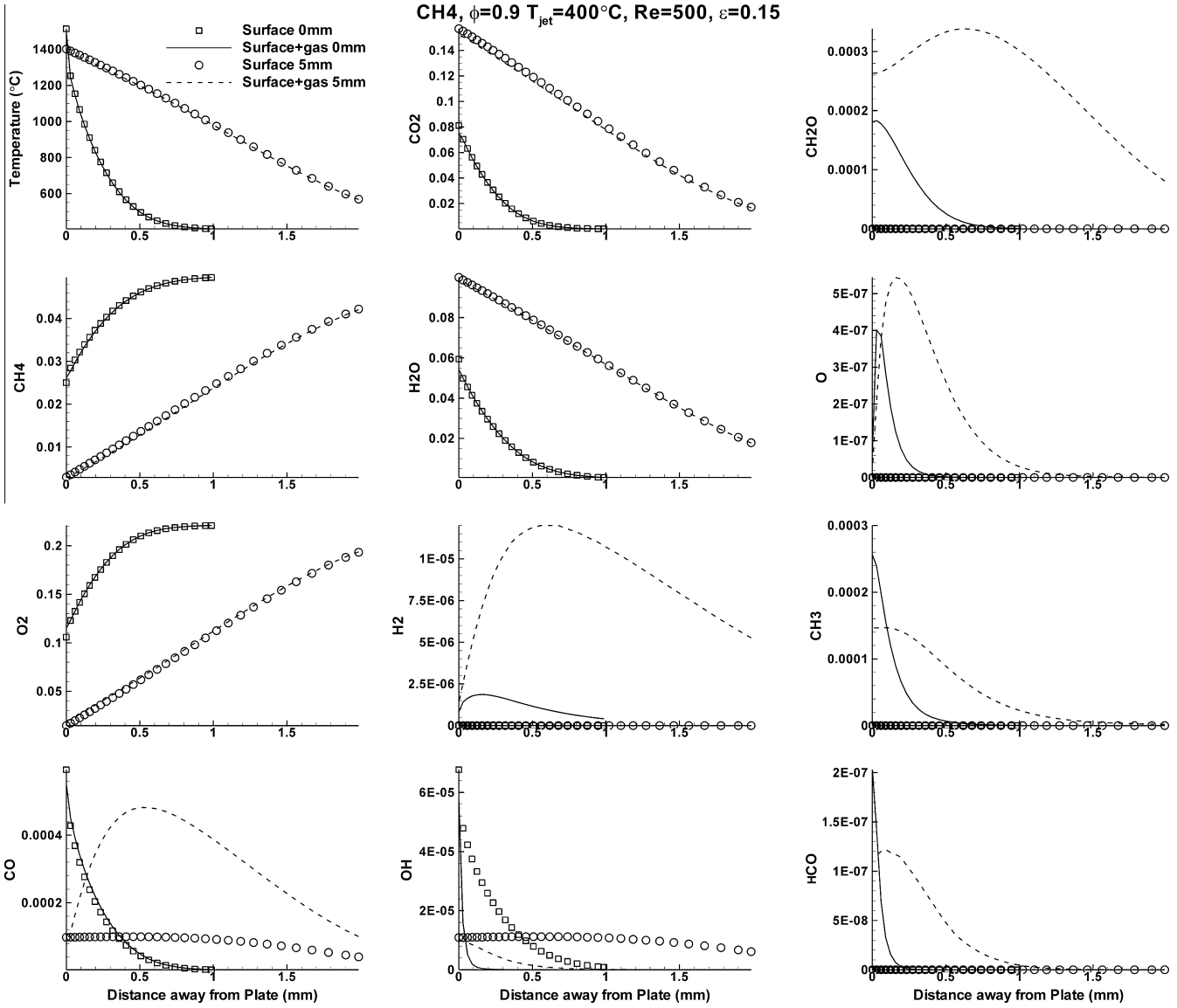

Fig. 11. Transverse profiles of temperature and species mass fraction computed for T_{jet} = 400 °C, Ø = 0.9 and Re = 500. Profiles are shown for two downstream locations (0 mm and 5 mm) using surface only or surface + gas reactions as marked on the inset.

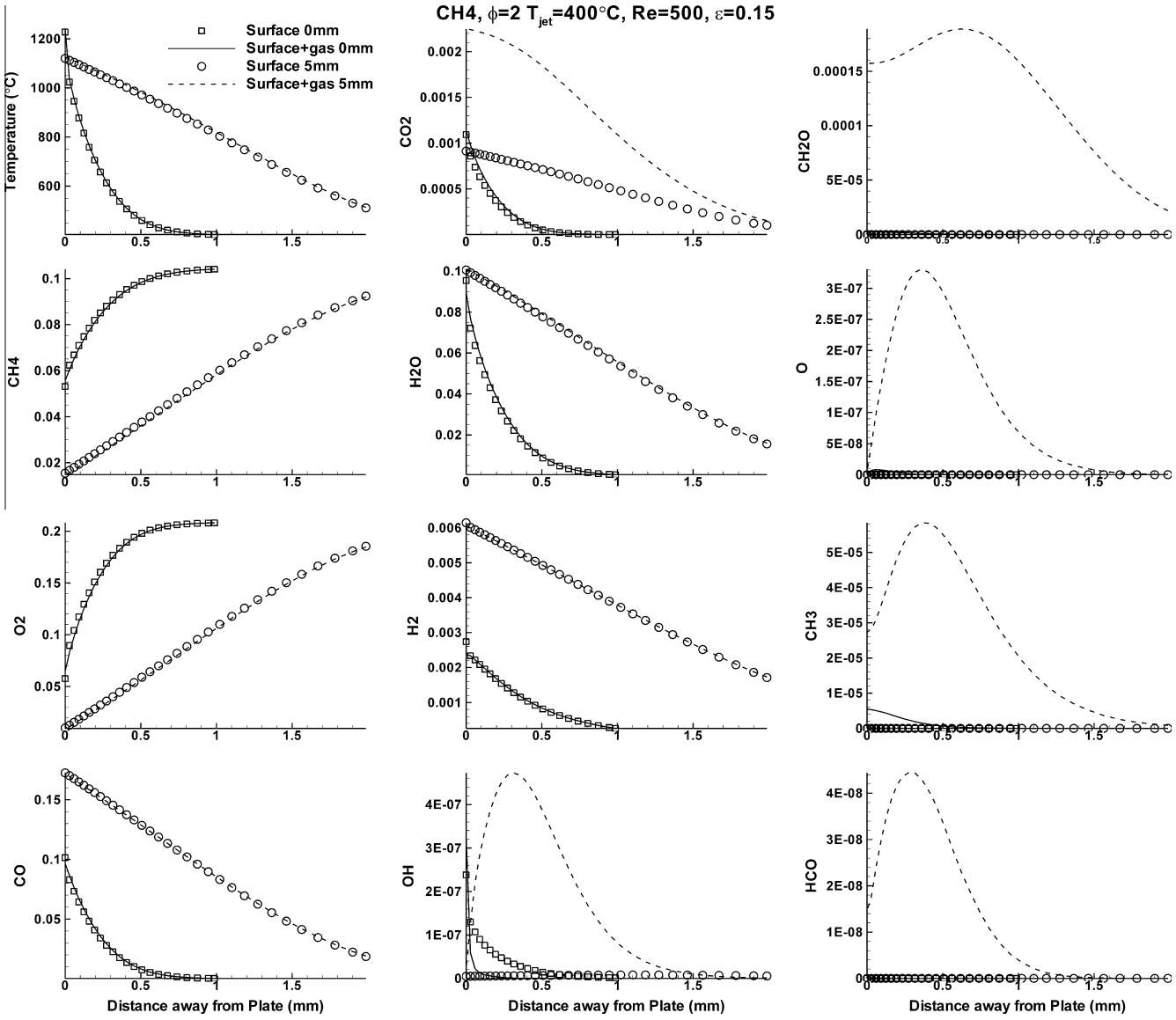

Fig. 12. Transverse profiles of temperature and species mass fraction computed for T_{jet} = 400 °C, Ø = 2 and Re = 500. Profiles are shown for two downstream locations (0 mm and 5 mm) using surface only or surface + gas reactions as marked on the inset.

highest on the plate's surface and this is almost entirely due to surface chemistry but further away from the plate, gas chemistry contributes to the destruction of OH as is evident from the profiles shown in Fig. 10.

This is confirmed from a comparison of the rates of production of OH across the boundary layer. At 5 mm from the leading edge, the net reaction rate for OH changes from $1.1e^{-8}$ kg/m^3 s to 0 kg/m^3 s across a 2.5 mm boundary layer using surface chemistry alone. With surface + gas chemistries at the same location the net reaction rates increases form -0.018 kg/m^3 s to 0 kg/m^3 s across a 0.25 mm boundary layer. This confirms that the OH which desorbs from the platinum by a set of surface reactions gets consumed by the gaseous reactions as it diffuses away from the surface into the boundary layer. It should be noted that the pattern described in Fig. 10 for the case of Ø = 0.9, T_{jet} = 27 °C, and Re = 500 is also relevant at higher Reynolds numbers with Ø = 0.9, T_{jet} = 27 °C, and Re = 1500 (not shown here).

Figure 11 shows computed profiles for the case where T_{jet} rises to 400 °C at Ø = 0.9 and Re = 500. The overall structure is very similar to the case shown in Fig. 10 for T_{jet} = 27 °C except for CO and CO_2 where the gas chemistry has more impact. The computed mass fractions of CO have increased significantly for the S + G case at 5 mm from the leading edge of the platinum. The higher temperature of the incoming mixture activates CO production due to gaseous reactions some 0.5 mm away from the plate where CH_2O is also formed in sizeable quantities. The computed profiles of CO_2 profiles show also a slight deviation due to the active gas chemistry.

For a richer incoming mixture with Ø = 2, T_{jet} = 400 °C, and Re = 500, Fig. 12 shows significant changes in the compositional structure compared to the case presented in Fig. 11 for Ø = 0.9. The mass fractions of CO and H_2 formed on the platinum increase by more than three orders of magnitude. Additionally, the overlap between the S and S + G profiles of H_2 and CO implies that surface chemistry is in control. The mass fraction of CO_2 decreases by a corresponding amount but the same cannot be said about H_2O which drops only slightly. The CO_2 levels decrease significantly and some active gas chemistry is evident at 5 mm from the leading edge increasing the peak CO_2 mass fraction from about 0.001 to 0.0022. The fact that H_2O does not decrease by an amount

corresponding to the increase in H_2 is largely due to lower mass fraction of OH obtained for this case. The increase in the mass fraction of H_2 is an artifact of the increased formation of H(s) on the surface due to the higher concentration of CH_4 in the mixture which then recombines to form H_2 through a series of surface reactions.

Albeit limited to methane for now, it is clear that a wealth of information can be gleaned from these detailed and computationally expensive calculations. While gaseous mechanisms for the remaining fuels (propane, butane and DME) may be made available, their detailed surface chemistry on platinum is severely lacking. Earlier calculations by Stefandis and Vlachos [23] and Karagiannidis et al. [26] used a single-step catalytic reaction for propane on platinum. There is an urgent need, therefore, to develop detailed catalytic mechanisms for the range of fuels studied here as well as others.

5. Conclusions

The experimental and numerical studies reported here confirm that the hetero–homogeneous interactions in the presence of platinum are complex and highly dependent on the fuel used as well as other parameters such as temperature, equivalence ratio and Reynolds number of the gaseous fuel–air mixture. The following conclusions are drawn:

- The peak temperature of the platinum surface, $T_{p,\max}$ increases with increasing Reynolds number for all four fuels studied here. However, the surface temperature peaks near stoichiometric for CNG–air mixtures whereas, for LPG, butane and DME fuels, $T_{p,\max}$ occurs at an equivalence ratio of about 1.5.
- The reactivity limits of the fuel–air mixtures are generally broader in the presence of platinum except for butane where the lean and rich reactive limits remained close to those of the gas phase. DME is the most reactive, decomposing on platinum as a pure fuel, followed by CNG and then LPG.
- Very good agreement is obtained between the calculated and measured temperatures over a range of conditions for CNG–air mixtures where T_{jet}, Re and Ø are varied. It is also found that the peak platinum temperature is largely unaffected by the gas-phase reactions.
- Combined gas and surface chemistries affect a few species such as CO, CO_2, H_2, and H_2O depending on the conditions (T_{jet}, Re and Ø) of the co-flowing mixture. Minor species such as CH_3, CH_2O, O, HCO, and OH are mainly controlled by gas-phase chemistry.

Acknowledgment

This research is supported by the Australian Research Council.

References

[1] C. Fernandez-Pello, Proc. Combust. Inst. 29 (2002) 883–899.
[2] D. Dunn-Rankin, E. Leal, D. Walther, Prog. Energy Combust. Sci. 31 (2005) 422–465.
[3] K. Fu, A.J. Knobloch, F.C. Martinez, D.C. Walther, C. Fernandez-Pello, A.P. Pisano, D. Liepmann, K. Miyasaka, K. Maruta, in: Design and Experimental Results of Small-Scale Rotary Engines, ASME International Mechanical Engineering Congress & Exposition, New York, November 11–16, 2001.
[4] J. Peirs, D. Reynaerts, F. Verplaestsen, J. Micromech. Microeng. 13 (2003) S190–S195.
[5] A.H. Epstein, S.D. Senturia, Science 276 (1997) 1211.
[6] A. Mehra, A.A. Ayon, I.A. Waitz, M.A. Scmidt, J. Microelectromech. Syst. 8 (1999) 152–160.
[7] C.M. Spadaccini, J. Peck, I.A. Waitz, J. Eng. Gas Turbines Power-Trans. ASME 129 (1999) 49–60.
[8] I.A. Waitz, G. Gauba, Y.S. Tzeng, J. Eng. Gas Turbines Power-Trans. ASME 120 (1998) 109–117.
[9] C.P. Chen, Y.C. Chao, C.Y. Wu, J.C. Lee, G.B. Chen, Combust. Sci. Technol. 178 (2006) 2039–2060.
[10] G.A. Boyarko, C.J. Sung, S.J. Schneider, Proc. Combust. Inst. 30 (2005) 2481–2488.
[11] D.A. Hickman, L.D. Schmidt, Science 259 (1993) 343–346.
[12] D.A. Hickman, L.D. Schmidt, AIChE J. 39 (1993) 1164–1177.
[13] K. Maruta, Proc. Combust. Inst. 33 (2011) 125–150.
[14] Y. Ju, K. Maruta, Prog. Energy Combust. Sci. (2011), in press, doi:10.1016/j.pecs.2011.03.001.
[15] H.F. Coward, P.G. Geust, J. Am. Chem. Soc. 49 (1927) 2479–2486.
[16] H.F. Coward, H.P. Greenwald, in: D. o. C. US Bureau of Mines, (Ed.), Technical Paper 427, 1928, pp. 1–28.
[17] G. Veser, L.D. Schmidt, AIChE J. 42 (1996) 1077–1087.
[18] W.R. Williams, M.T. Stenzel, X. Song, L.D. Schmidt, Combust. Flame 84 (1991) 277–291.
[19] H.M. Kim, H. Enomoto, H. Kato, M. Tsue, M. Kono, Combust. Sci. Technol. 128 (1997) 197–213.
[20] X. Song, W.R. Williams, L.D. Schmidt, R. Aris, Symp. (Int.) Combust. 23 (1991) 1129–1137.
[21] Y. Ghermay, J. Mantzaras, R. Bombach, Proc. Combust. Inst. 33 (2011) 1827–1835.
[22] S. Karagiannidis, J. Mantzaras, R. Bombach, S. Schenker, K. Boulouchos, Proc. Combust. Inst. 32 (2009) 1947–1955.
[23] G.D. Stefandis, D.G. Vlachos, Ind. Eng. Chem. Res. 48 (2009) 5962–5968.
[24] G.B. Chen, C.P. Chen, C.Y. Wu, Y.C. Chao, Appl. Catal. A 332 (2007) 89–97.
[25] U. Dogwiler, P. Benz, J. Mantzaras, Combust. Flame 119 (1999) 455–472.
[26] S. Karagiannidis, J. Mantzaras, K. Boulouchos, Proc. Combust. Inst. 33 (2011) 3241–3249.
[27] O. Deutschmann, R. Schmidt, F. Beherendt, J. Warnatz, Proc. Combust. Inst. 26 (1996) 1747–1754.
[28] K. Maruta, K. Takeda, J. Ahn, K. Borer, L. Stizki, P.D. Ronney, O. Deutschmann, Proc. Combust. Inst. 29 (2002) 957–963.
[29] S.A. Smyth, K.T. Christensen, D.C. Kyritsis, Proc. Combust. Inst. 32 (2009) 3035–3042.
[30] Fluent (version 6.3.26), <http://www.fluent.com> (20.01.11).
[31] A. Kazakov, M. Frenklach, <http://www.me.berkeley.edu/drm/> (06.04.11).
[32] O. Deutschmann, L.I. Maier, U. Riedel, A.H. Stroemman, R.W. Dibble, Catal. Today 59 (2000) 141–150.
[33] R.L. Gordon, A.R. Masri, S.B. Pope, G.M. Goldin, Combust. Theory Modell. 11 (2007) 351–376.
[34] Emissivity of Platinum, <http://www.platinummetalsreview.com/jmpgm/data/displayFunctionalGraph.do;jsessionid=40584A142C4D91784CC7BD150B2DF3A4?record=1219&attribute=154&database=cesdatabase> (11.04.11).
[35] M.G. Zabetakis, Flammability Characteristics of Combustible Gases and Vapors, Bureau of Mines, Alaska, 1665a, pp. 22, 23, 70.
[36] J. Ahn, C. Eastwood, L. stizki, P.D. Ronney, Proc. Combust. Inst. 30 (2005) 2463–2472.
[37] P.A. Bui, D.G. Vlachos, P.R. Westmoreland, Proc. Combust. Inst. 26 (1996) 1763–1770.